SUPPLEMENTARY INFORMATION

Synthesis of Carbon Dots from Spent Coffee Grounds: Transforming Waste into Potential Biomedical Tools

Yingru Zhou [a,b], Adalberto Camisasca [a], Sofia Dominguez-Gil [a], Michał Bartkowski [a], Keith D. Rochfort [b, c], Martina Piletti [d], Anita White [b,c], Dorottya Krizsan [e], Rob O'Connor [f], Susan J. Quinn [e], Daniela Iacopino [d], Alex J. Eustace *[b,c], Silvia Giordani *[a,b]

[a] Y. Zhou, Dr. A. Camisasca, Dr. S. Dominguez-Gil, Dr. M. Bartkowski, Prof. S. Giordani.
School of Chemical Science
Dublin City University
Glasnevin, Dublin, Ireland
E-mail: silvia.giordani@dcu.ie

[b] Y. Zhou, Dr. K.D. Rochfort, A. White, Dr. A. J. Eustace, Prof. S. Giordani.
Life Sciences Institute
Dublin City University
Glasnevin, Dublin, Ireland

[c] Dr. K.D. Rochfort, A. White, Dr. A. J. Eustace.
School of Biotechnology
Dublin City University
Glasnevin, Dublin, Ireland
E-mail: alex.eustace@dcu.ie

[d] M. Piletti, Dr. D. Iacopino.
Tyndall National Institute
University College Cork
Cork, Ireland

[e] Dr. D. Krizsan, Prof. S. J. Quinn.
School of Chemistry
University College Dublin
Belfield, Dublin, Ireland

[f] Dr. R. O'Connor
School of Physical Sciences,
Dublin City University
Glasnevin, Dublin, Ireland

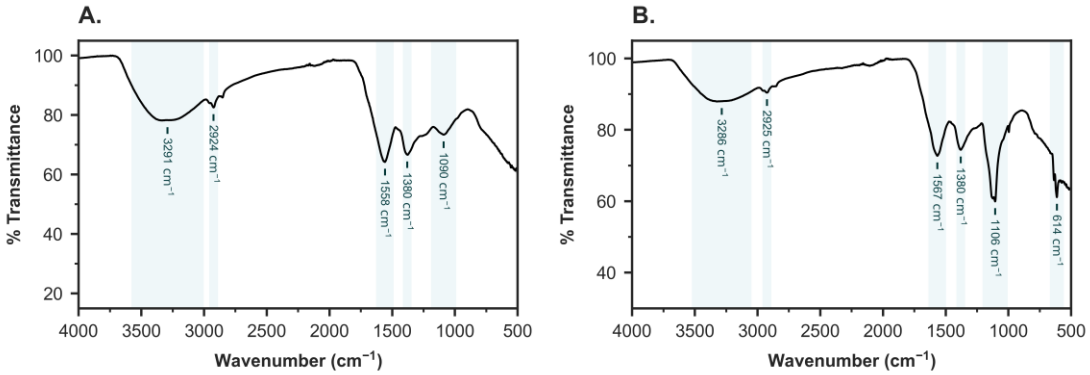

Fig S1. ATR-FTIR spectra of **A.** D-LAV-CDs and **B.** D-KEN-CDs. Prominent bands have been highlighted and labelled with the corresponding wavenumber.

Tab S1. Wavenumbers corresponding to key functional groups observed in the ATR-FTIR spectra of AP-LAV-CDs, D-LAV -CDs and D-KEN-CDs. The symbol *v* denotes stretching vibrations and *n.p.* denotes 'not present'.

	AP-LAV-CDs (cm^{-1})	**D-LAV-CDs (cm^{-1})**	**D-KEN-CDs (cm^{-1})**
***v*(OH)**	3322	3291	3286
sp^3 *v*(C-H)	*n.p.*	2924	2925
***v*(C=O)**	1598	1558	1567
***v*(C=C)**	1402	1380	1380
***v*(C-O-C)**	1099	1106	1106
fingerprint region	611	*n.p.*	614

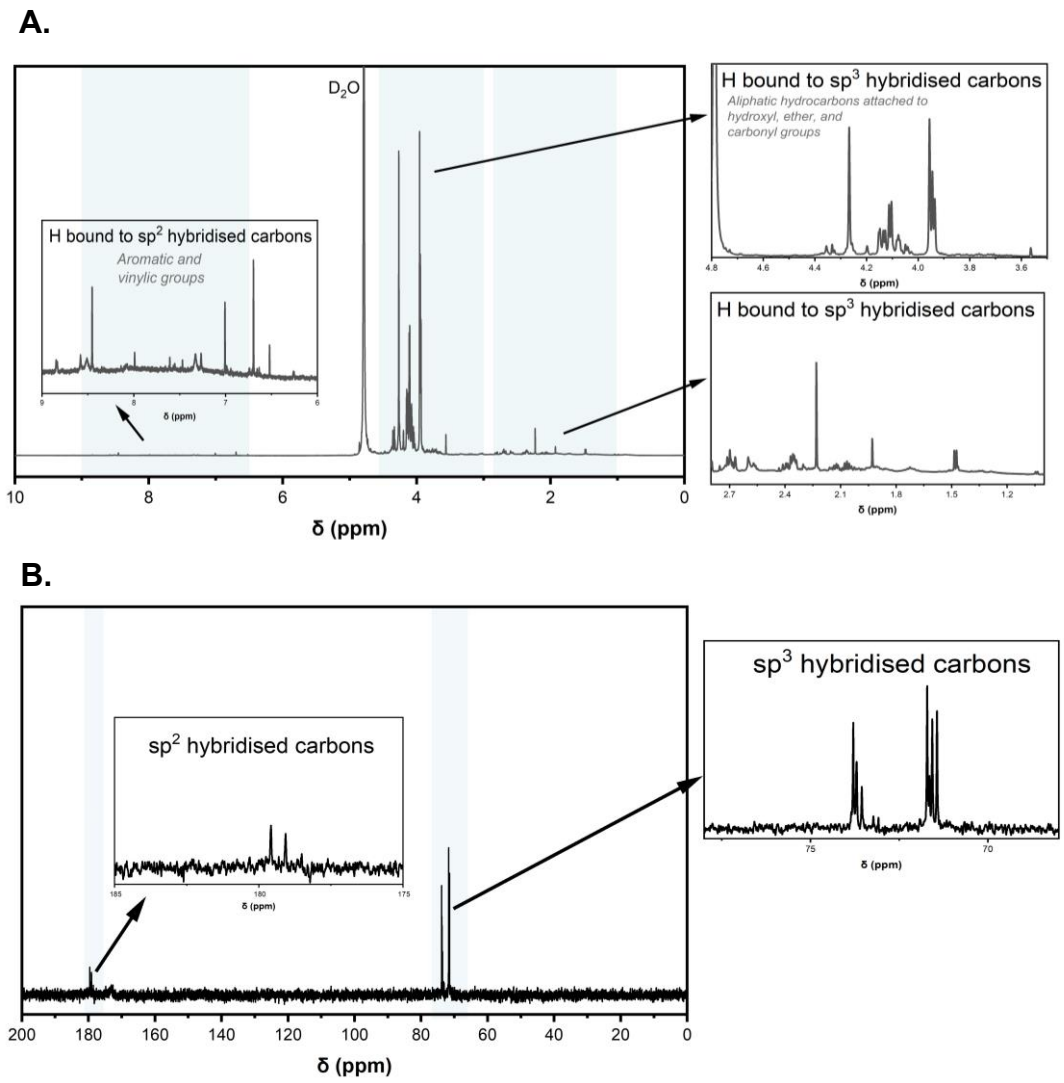

Fig S2. NMR spectra of AP-LAV-CDs. **A.** ^{1}H NMR spectrum (1024 scans), showing signals from sp^3- and sp^2-hybridised carbon atoms. *Insets*: Expanded regions from 9-6 ppm, 4.8-4.5 ppm, and 2.8-1 ppm. **B.** ^{13}C NMR spectrum (4096 scans), displaying sp^3- and sp^2-hybridised carbon atoms, with peaks around 70 ppm and 180 ppm, respectively. *Inset*: Expanded regions from 185-175 ppm and 78-68 ppm.

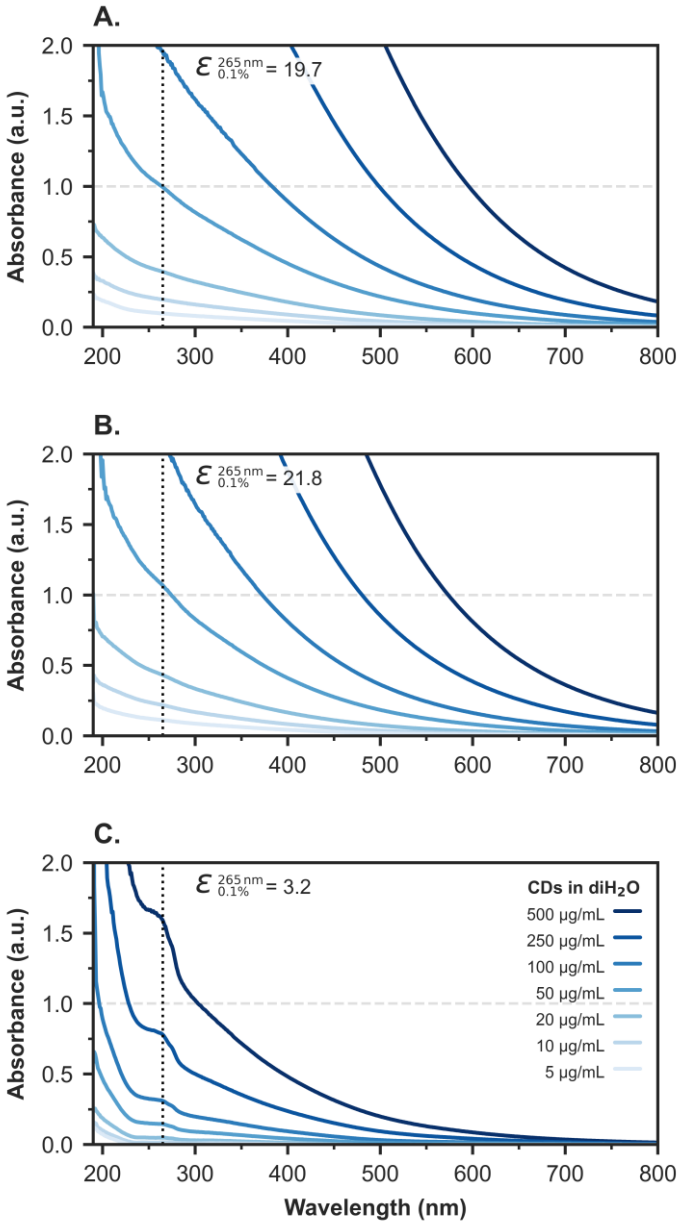

Fig S3. UV-Vis absorption spectra of **A.** D-LAV-CDs, **B.** D-KEN-CDs and **C.** AP-LAV-CDs dispersed in diH_2O at 5, 10, 20, 50, 100, 250 and 500 µg/mL. The 0.1% excitation coefficient calculated at 265 nm for concentrations ≤ 50 µg/mL is shown.

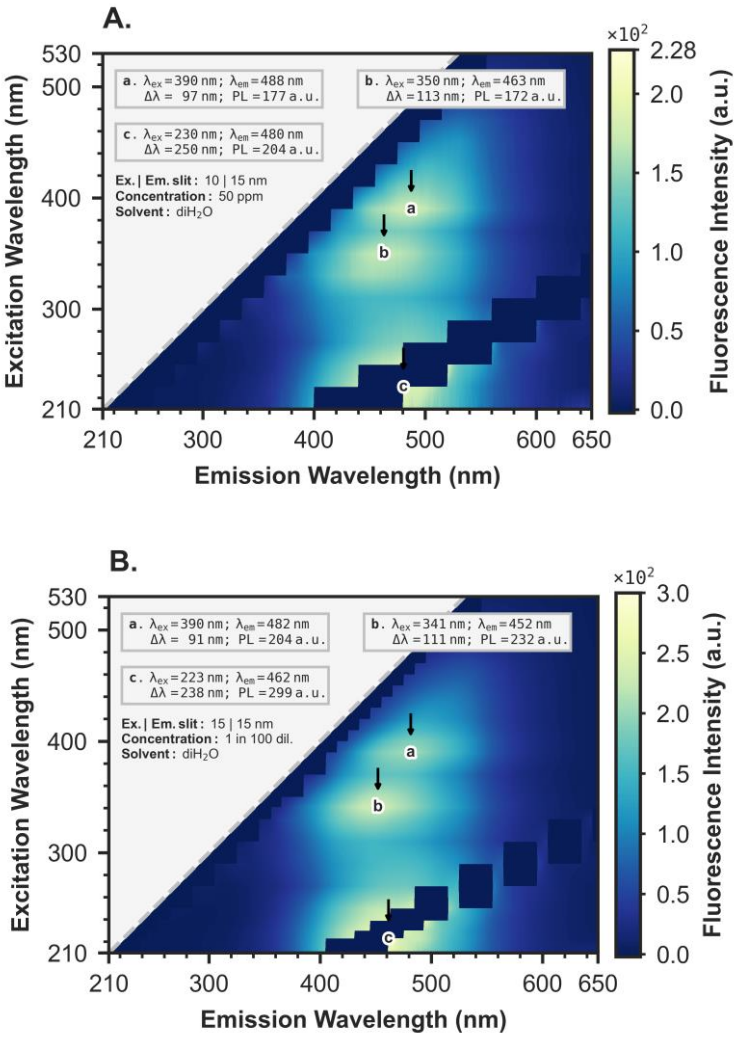

Fig S4. Fluorescence excitation emission matrix (EEM) spectra of **A.** D-KEN-CDs and **B.** D-LAV-CDs. Relevant experimental conditions have been noted, and significant emission regions have been annotated as **a**, **b** & **c**, with the excitation wavelength (λ_{ex}), emission wavelength (λ_{em}) and Stokes shift ($\Delta\lambda$) at the point of highest intensity emission (PL). First- and second-order Rayleigh scattering signals have been excluded (dark spaces).

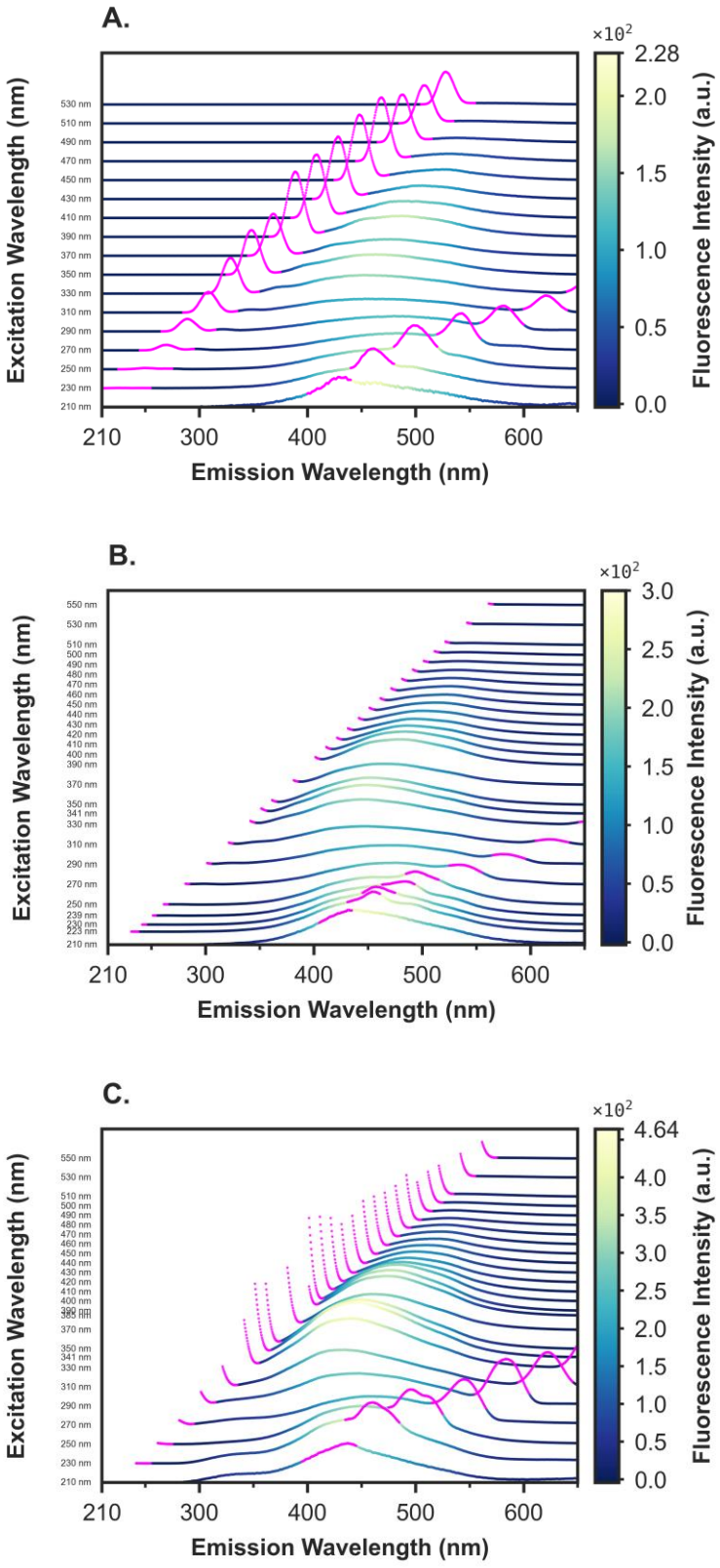

Fig S5. Fluorescence emission spectroscopy data of **A.** D-KEN-CDs; **B.** D-LAV-CDs; and **C.** AP-LAV-CDs visualised in an alternative approach to the EEM. First- and second-order Rayleigh scattering signals have been highlighted in pink.

Tab S2. Summary of SCG-derived CDs' fluorescence emission results; included are the excitation wavelength (λ_{ex}), emission wavelength (λ_{em}), Stokes shift ($\Delta\lambda$), and highest intensity emission (PL) for the annotated regions **a**, **b**, and **c** in the respective fluorescence excitation emission matrix (EEM) spectra of AP-LAV-CDs, D-LAV-CDs and D-KEN-CDs.

Region	Parameter	AP-LAV-CDs	D-LAV-CDs	D-KEN -CDs
a	**λ_{ex} (nm)**	390	390	390
a	**λ_{em} (nm)**	478	482	488
a	**$\Delta\lambda$ (nm)**	88	91	97
a	**PL (a.u.)**	345	204	177
b	**λ_{ex} (nm)**	341	341	350
b	**λ_{em} (nm)**	445	452	463
b	**$\Delta\lambda$ (nm)**	104	111	113
b	**PL (a.u.)**	462	232	172
c	**λ_{ex} (nm)**	230	223	230
c	**λ_{em} (nm)**	434	462	480
c	**$\Delta\lambda$ (nm)**	204	238	250
c	**PL (a.u.)**	368	299	204

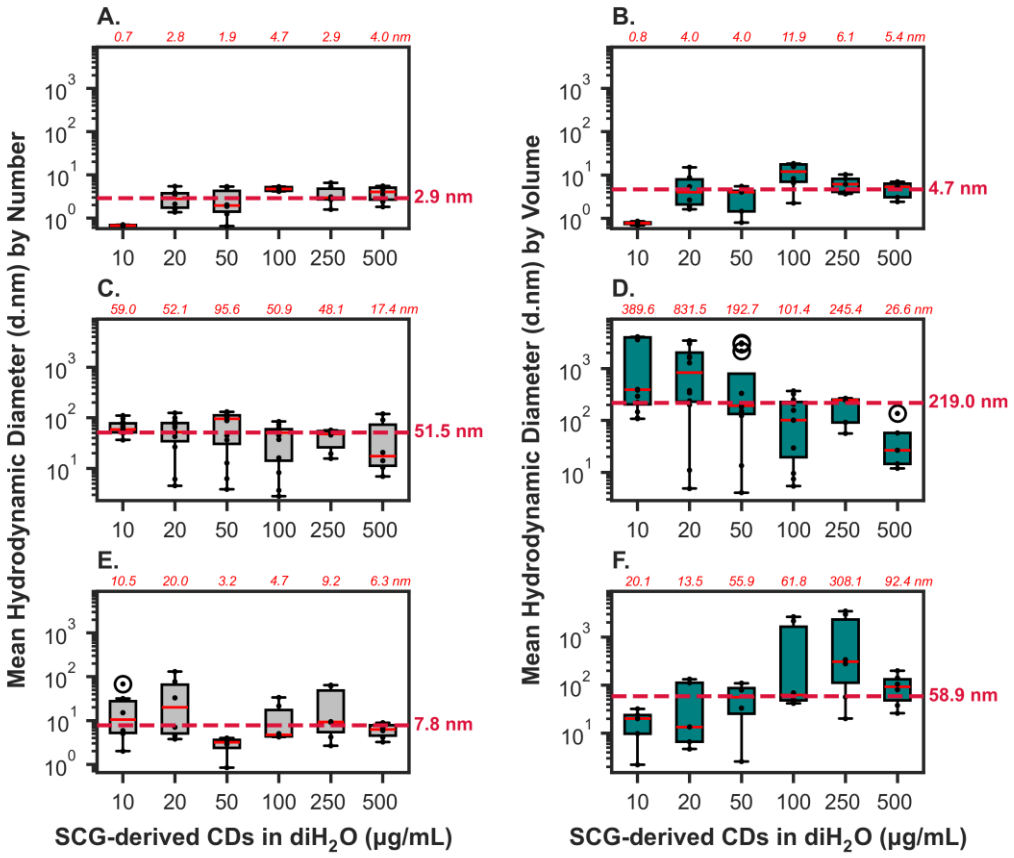

Fig S6. DLS hydrodynamic diameter (d.nm) data of **A.** & **B.** AP-LAV-CDs represented by number and by volume, respectively; **C.** & **D.** D-LAV-CDs represented by number and by volume, respectively; **E.** & **F.** D-KEN-CDs represented by number and by volume, respectively. The SCG-derived CDs have been dispersed in diH_2O at 10, 20, 50, 100, 250 and 500 µg/mL, and the data represents $n \geq 6$ runs. The data for each concentration has been represented as a box and whisker plot. The individual median values for each concentration, as well as the overall median across all concentrations, have been annotated in red.

Tab S3. DLS mean hydrodynamic diameter (d.nm) data for AP-LAV-CDs, D-LAV-CDs, and D-KEN-CDs, represented by number distribution. The SCG-derived CDs were dispersed in diH_2O at concentrations of 10, 20, 50, 100, 250, and 500 µg/mL. Data is presented as mean ± standard deviation from $n \geq 6$ runs for each concentration.

Concentration (µg/mL)	AP-LAV-CDs (nm)	D-LAV-CDs (nm)	D-KEN-CDs (nm)
10	0.7 ± 0.1	66.8 ± 22.4	21.3 ± 25.4
20	3.0 ± 1.6	57.1 ± 37.5	42.7 ± 51.6
50	2.7 ± 2.0	73.5 ± 49.1	2.8 ± 1.4
100	4.7 ± 0.5	42.3 ± 28.4	12.2 ± 12.5
250	3.7 ± 1.9	40.7 ± 18.5	25.1 ± 29.2
500	3.8 ± 1.5	43.8 ± 48.7	6.2 ± 2.2

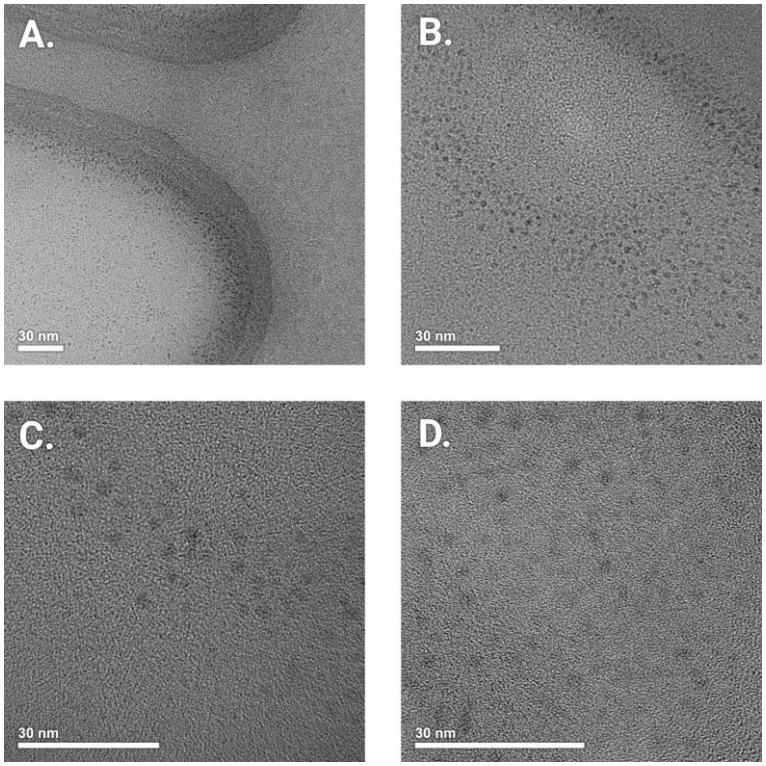

Fig S7. TEM images of AP-LAV-CDs at four different magnifications (**A.** 80,000x, **B.** 150,000x, **C.** 250,000x, and **D.** 300,000x); all images have been fitted with a 30 nm scale bar.

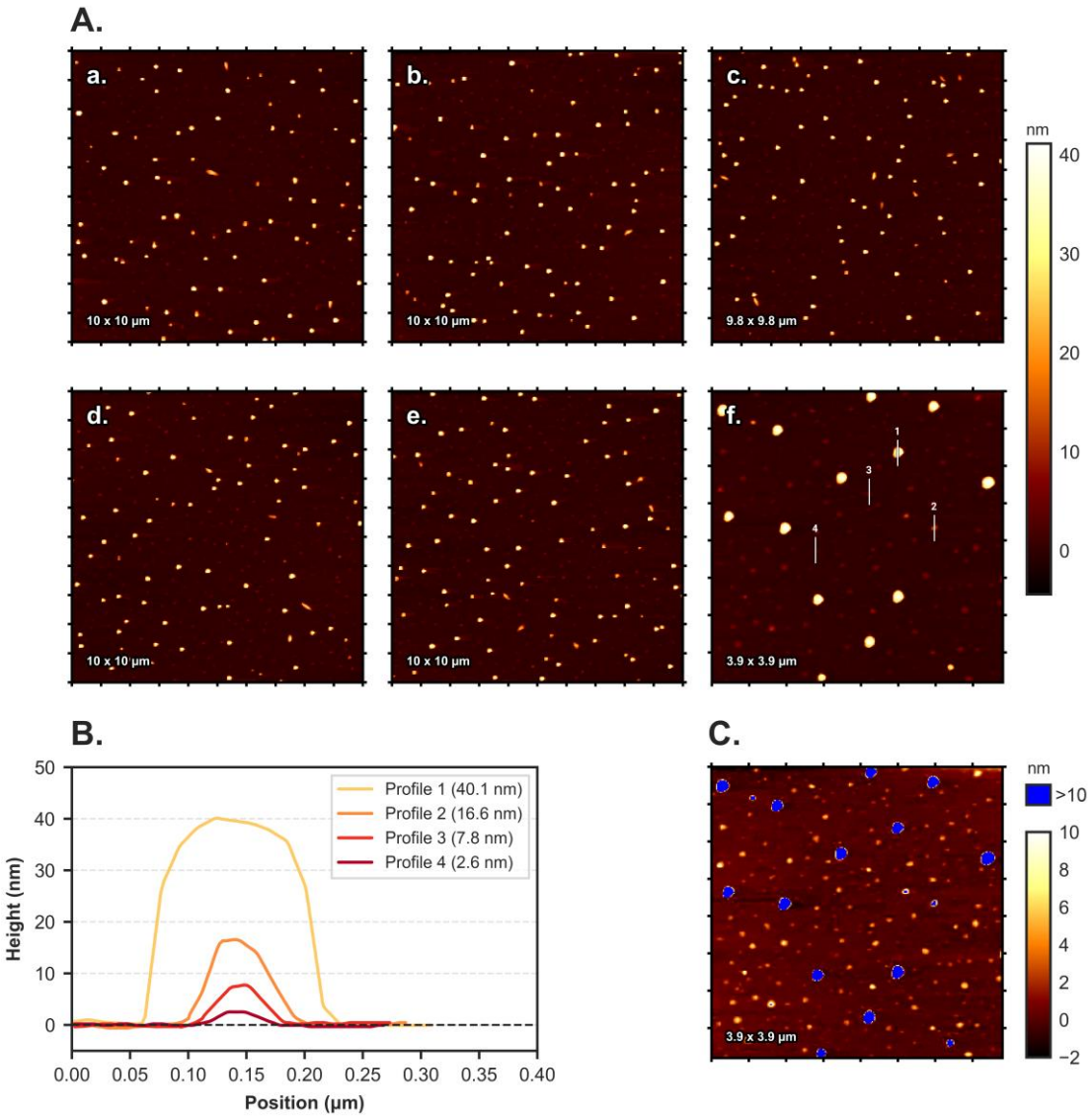

Fig S8. A. AFM images of AP-LAV-CDs at different scan sizes. All AFM images **a.-f.** have been represented using a common colour-scale for comparative purposes. **B.** Line profiles 1 to 4, respectively marked in subfigure **f.**, highlighting NPs of different heights; the maximum height of each line profile is provided in its respective legend entry. **C.** AFM image **f.** with the colour-scale normalised to a maximum height of 10 nm to better visualise small (< 10 nm height) NPs. Height data clipping > 10 nm has been highlighted in blue.

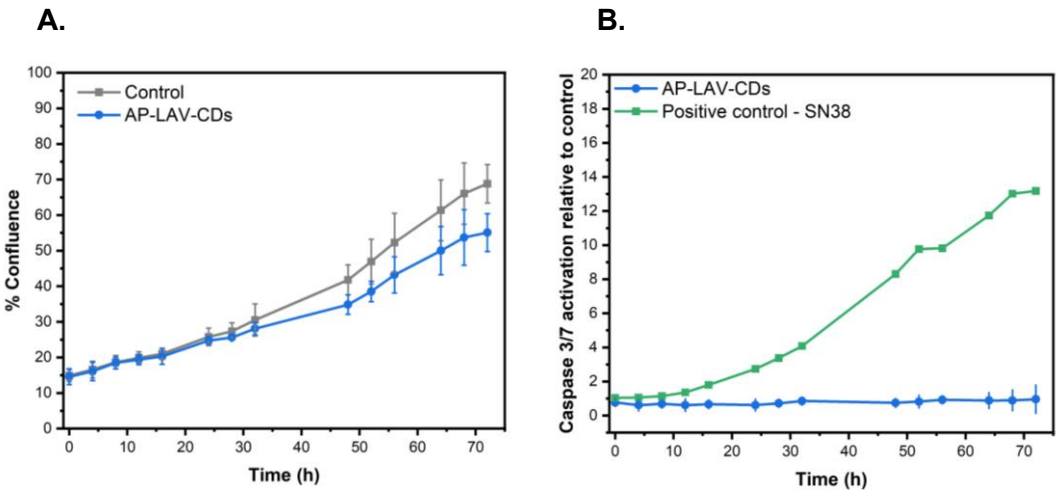

Fig S9. Apoptosis study on AP-LAV-CDs with InCucyte® Live-Cell Analysis System **A.** Cell confluency of CAL-51 cells treated with 250 µg/mL AP-LAV-CDs; **B.** Apoptosis signal in CAL-51 cells treated with 250 µg/mL AP-LAV-CDs compared to the positive control SN38. Data is normalized to untreated controls to account for baseline apoptosis levels.

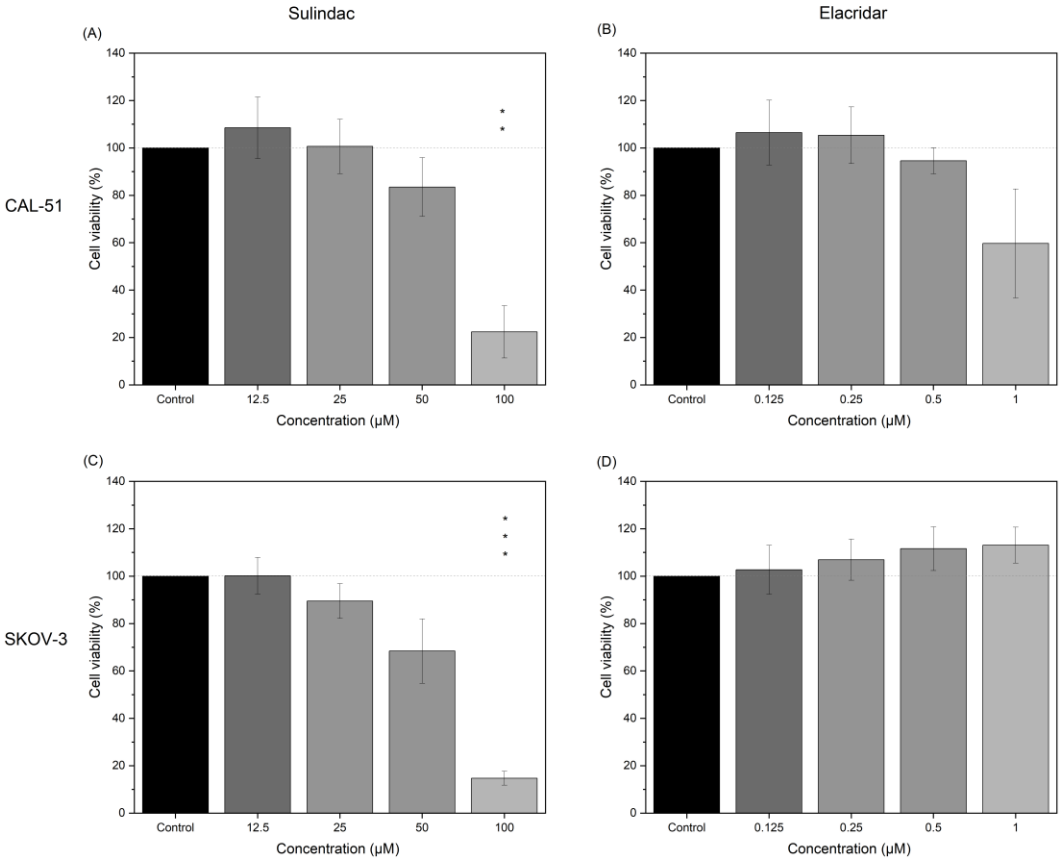

Fig S10. Cellular viability of **A.** CAL-51 cells treated with sulindac; **B.** CAL-51 cells treated with elacridar; **C.** SKOV-3 cells treated with sulindac; and **D.** SKOV-3 cells treated with elacridar. Cells were exposed to sulindac at concentrations of 0 (control), 12.5, 25, 50, and 100 μM, and to elacridar at concentrations of 0 (control), 0.125, 0.25, 0.50, and 1 μM, for 120 h. Data represent the mean ± standard deviation of three replicates.